applied optics

Elimination of the field-dependent aberrations of the JWST-like space telescopes in the multi-field fine-phasing process

Guohao Ju,[1,2,*] Changxiang Yan,[1] and Zhiyuan Gu[1]

[1]Changchun Institute of Optics, Fine Mechanics and Physics, Chinese Academy of Sciences, Changchun, Jilin 130033, China
[2]University of Chinese Academy of Sciences, Beijing 100049, China
*Corresponding author: juguohao123@163.com

Received 26 December 2016; revised 17 February 2017; accepted 27 February 2017; posted 1 March 2017 (Doc. ID 283630); published 24 March 2017

This paper investigates the alignment strategies for eliminating the field-dependent aberrations of the class of large three-mirror anastigmatic (TMA) space telescopes with a segmented primary mirror (PM) like the James Webb Space Telescope (JWST) in the multi-field fine-phasing process based on the framework of nodal aberration theory. During the single-field (on-axis field) fine-phasing process, the individual segment tip, tilt, and piston errors, as well as the de-space of the secondary mirror, are well corrected, and the PM is also adjusted to compensate for those aberrations induced by the misalignments of other mirrors at the center of the science field of view. However, interrogating off-axis field points can reveal the presence of large wavefront errors due to mirror misalignments. Eliminating these field-dependent aberrations is the main goal of the multi-field fine-phasing process. This paper first presents an analytic study on an established alignment strategy used for eliminating the field-dependent aberrations. While it is demonstrated that this alignment strategy has the ability to reduce the field dependency of the wavefront errors, it will, however, also be revealed that this strategy still exhibits some problems, and its alignment efficiency is low. Then, a new alignment strategy with higher alignment efficiency is further proposed. Detailed simulations with a TMA telescope that has similar parameters with the JWST are performed to illustrate the efficiency and rationality of the proposed strategy. This work can not only contribute to an in-depth understanding of the multi-field fine-phasing process, but also present a possibility to improve the efficiency of this process.

OCIS codes: (110.6770) Telescopes; (080.1010) Aberrations (global); (220.1140) Alignment; (220.1080) Active or adaptive optics.

https://doi.org/10.1364/AO.56.002724

1. INTRODUCTION

A scientific successor to the Hubble Space Telescope (HST) [1] and the Space Infrared Telescope Facility (SIRTF) [2], the James Webb Space Telescope (JWST) is a 6 m class infrared (IR) telescope, which will be located in an orbit near the second Lagrange point (L2). The main goal of it is to study and answer some fundamental astrophysical questions ranging from the formation and structure of the universe to the origin of planetary systems and the origins of life [3]. JWST represents a new generation class of space telescopes, i.e., the class of large three-mirror anastigmatic (TMA) space telescopes with a segmented primary mirror (PM). This class of telescope can not only achieve a high light collecting efficiency and imaging resolution, but also provide near diffraction-limited imaging quality over a relatively large field of view (FOV).

One of the main characteristics of this class of space telescopes like JWST is that they are deployable with a segmented PM and, therefore, must be completely aligned and phased after launch. This is achieved through wavefront sensing and control (WS&C), which consists of a series of commissioning steps [4–6]. The multi-field fine-phasing process follows the single-field (on-axis field) fine-phasing process. During the single-field fine-phasing process, the individual segment tip, tilt, and piston errors as well as the de-spacing of the secondary mirror (SM) are well corrected. Besides, the PM is also adjusted to compensate for those aberrations induced by SM misalignments at the center of the science FOV. Therefore, the aberrations of the on-axis field point are all well corrected. However, interrogating off-axis field points can reveal the presence of large wavefront errors (WFEs) due to mirror misalignments, i.e., there still exist some field-dependent aberrations in the system after the single-field fine-phasing process. Eliminating these aberrations is the main goal of the multi-field fine-phasing process, and some alignment strategies are needed to accomplish the task.

An established alignment strategy that is currently for the multi-field fine-phasing process directly utilizes the degrees of freedom of the SM to eliminate those field-dependent aberrations [4,7] (in this paper, we refer to this strategy as "the current strategy"). A numerical method is utilized to obtain the corrective SM moves that are required to minimize the field dependency of the WFEs. The specific algorithm is presented below [4,7]. First, WFEs at four corners of a rectangular field and the on-axis field point are recovered using the phase retrieval method, discarding all but the two field-dependent aberration terms (astigmatism and focus). Then, a linear model is applied to estimate the corrective SM modes based on these wavefront measurements, since ray-trace data shows that the field dependency of the WFEs consists of a strong linear function of the SM misalignment terms. Detailed information about this linear model is presented in Ref. [7].

The practicability of the numerical method used in this current alignment strategy for obtaining the corrective SM moves has been demonstrated, however, the numerical method cannot contribute to an in-depth understanding of this current alignment strategy. It cannot provide us with any insight into the interactions between the field-dependent aberrations and the SM degrees of freedom. Besides, some basic questions about this alignment strategy also need to be answered. For example, we still lack the knowledge of the minimum number of field points, which are enough for us to eliminate the field-dependent aberrations using this strategy. This knowledge is important because it can provide a theoretical basis for us to reduce the number of the field points for wavefront measurements and facilitate the multi-field fine-phasing process. Besides, the positions of the five field points used for wavefront measurement are fixed in the field, because the sensitivities of the field-dependent aberrations to SM misalignments used in the linear numerical model are unique for a certain field point. However, in practice, it is very likely that no suitable guide star is located at the designated field points. In this case, we need to adjust the boresight, which can increase the uncertainty and inefficiency of the WS&C commissioning process. Therefore, it is very convenient that wavefront measurements at several arbitrary field points can be used for eliminating the field-dependent aberrations.

Furthermore, there still exist some other deep-rooted problems with the efficiency of the current strategy. The current strategy only concentrates on those field-dependent aberrations and directly uses the SM moves to eliminate them. However, a large field-constant aberration can be reintroduced into the system. Consequently, once the SM corrections are applied, the PM must be adjusted to reestablish an acceptable wavefront on-axis, which, unfortunately, can further introduce some field-dependent aberrations. Therefore, quite a lot of iterations may be required to achieve the adequate alignment of the system, and the alignment efficiency of the current alignment strategy is low. To improve the efficiency of the multi-field fine-phasing process, we need to propose an alignment strategy that can not only eliminate the field-dependent aberrations, but also maintain an acceptable wavefront on axis, i.e., the field-dependent aberrations and the field-constant aberrations induced by misalignments can be controlled at the same time.

Nodal aberration theory (NAT), developed by Shack and Thompson [8] and Thompson [9–13], is a powerful tool in investigating the aberration fields of optical systems without rotational symmetry. Schmid *et al.* [14] utilized NAT to study the misalignment-induced nodal aberration fields in two-mirror astronomical telescopes (especially Ritchey Chretien telescopes) and explained why the alignment of a large telescope based on axial imagery is insufficient. Thompson *et al.* [15] used NAT to describe the aberration field dependencies that arise in the presence of misalignments for TMA telescopes, and it is shown that the performance of TMA telescopes is dominated by the field-constant third-order coma, which can commonly be seen in two-mirror Ritchey Chretien telescopes, and the field-linear, field-asymmetric, third-order astigmatism. Schmid *et al.* [16] and Fuerschbach *et al.* [17,18] extended NAT to include freeform surfaces and illustrated that when the freeform surface is located away from the aperture stop, its net aberration contribution will become field dependent, and many aberration components each having a unique field dependence may arise. Recently, Ju *et al.* [19] further presented an in-depth and systematic discussion on the aberration fields of off-axis astronomical telescopes with an offset pupil induced by lateral misalignments based on NAT and provided some valuable insights into the alignment and active compensation and alignment of off-axis telescopes, according to the knowledge of the misalignment-induced aberrations.

On the other hand, NAT can also be used to develop specific and deterministic strategies for the alignment and active alignment of large astronomical telescopes. Ju *et al.* [20] quantified the effect of the trefoil deformation in an optical surface located away from the aperture stop and decentered from the optical axis based on NAT and developed an analytic strategy to quantitatively separate the effects of astigmatic and trefoil figure errors and misalignments for two-mirror astronomical telescopes. Gu *et al.* [21] applied third-order and fifth-order alignment models based on NAT to the alignment of TMA telescopes, respectively, and showed that the fifth-order alignment model has a higher computation accuracy. While the JWST-like space telescopes are essentially TMA telescopes, the alignment process of this class of telescope with a segmented PM is quite different from those with a monolithic PM. Consequently, the alignment strategies needed to eliminate the field-dependent aberrations in the multi-field fine-phasing process are also different.

In this paper, we first describe the aberration condition of the JWST-like space telescopes before the multi-field fine-phasing process to help understand the alignment strategies that will be discussed in this work. On one hand, we show that the main field-dependent aberrations are astigmatism and medial focal surface; on the other hand, we point out that the primary and secondary mirrors are in a compensated state for the coma aberration field. Then, we present an analytic study on the current alignment strategy for eliminating the main field-dependent aberrations. Specifically, we analytically derive the sensitivities of the field-dependent aberrations to the SM misalignments and propose an analytic method for determining the corrective SM modes for reducing the field dependency of the WFEs induced by misalignments. Monte Carlo simulations demonstrate that this strategy can greatly

reduce the field dependency of theWFEs. However, we also point out that there are some deep-rooted problems with this alignment strategy, and its alignment efficiency is low. A new alignment strategy is further proposed to improve the alignment efficiency of the multi-field fine-phasing process. Detailed simulations are conducted to demonstrate the efficiency of the proposed strategy. Some deep discussions are also presented to further illustrate the rationality of this strategy.

This paper is organized as follows: in Section 2, we describe the aberration condition of the JWST-like space telescopes before the multi-field fine-phasing process. In Section 3, we present an analytic study of the current alignment strategy for eliminating the field-dependent aberrations. In Section 4, we reveal the problem of the current alignment strategy and propose a new alignment strategy with higher efficiency. In Section 5, we summarize and conclude the paper.

2. ABERRATION CONDITION OF THE JWST-LIKE SPACE TELESCOPES BEFORE THE MULTI-FIELD FINE-PHASING PROCESS

The multi-field fine-phasing process follows the single-field fine-phasing process. One premise of this work is that after the single-field fine-phasing process, the aberrations of the on-axis field points are well corrected. In this case, on one hand, we can consider that the individual segment tip, tilt, and piston errors as well as the despacing of the SMs are well corrected. On the other hand, we should also note that if the SM is misaligned (either in position or orientation), it will create WFEs measured at the center FOV. This further indicates that during the single-field fine-phasing process, the PM is also adjusted to compensate for those aberrations induced by SM misalignments at the center FOV. However, some field-dependent aberrations still exist in the system due to mirror misalignments, and interrogating off-axis field points can reveal the presence of large WFEs. Eliminating these field-dependent aberrations is the main goal of the multi-field fine-phasing process.

In this section, we present a qualitative description of the field dependencies of three dominant aberrations of the JWST-like space telescopes before the multi-field fine-phasing process. On one hand, we will show that astigmatism and medial focal surface are the dominant field-dependent aberrations that need to be eliminated in this process. On the other hand, by discussing the coma aberration field, we will reveal the fact that the primary and secondary mirrors are in a compensated state for the coma aberration field. This knowledge is very important for understanding the work presented in the later parts of this paper.

A. Astigmatic Aberration Field

In the presence of misalignments, according to NAT, the astigmatic aberration field can be given by [10,15]

$$W_{\mathrm{AST}} = \frac{1}{2}\sum_j W_{222j}(\vec{H} - \vec{\sigma}_j)^2 \cdot \vec{\rho}^2 = \left(\frac{1}{2}W_{222}\vec{H}^2 - \vec{A}_{222}\vec{H} + \frac{1}{2}\vec{B}^2_{222}\right)\cdot\vec{\rho}^2, \quad (1)$$

where the subscript j is the surface number, W_{222j} is the astigmatic aberration coefficient for surface j, $\vec{H}$ is the vector that locates the image point of interest in the focal plane, $\vec{\rho}$ is the aperture vector in the exit pupil, and $\vec{\sigma}_j$ locates the shifted aberration field center for each surface. $W_{222} \equiv \sum_j W_{222j}$, representing the total astigmatism aberration coefficient. For TMA telescopes, which are typically by design corrected for the third-order astigmatism, we can consider $W_{222} \approx 0$. $\vec{A}_{222}$ and $\vec{B}^2_{222}$ are two unnormalized displacement vectors, given by

$$\vec{A}_{222} = \sum_j W_{222j}\vec{\sigma}_j, \qquad \vec{B}^2_{222} = \sum_j W_{222j}\vec{\sigma}^2_j. \quad (2)$$

In general, for misalignment level perturbations, the magnitude of $\vec{B}^2_{222}$ is proportional to the misalignment squared, and we can consider $\vec{B}^2_{222} \approx \vec{0}$. Therefore, Eq. (1) can be rewritten as

$$W_{\mathrm{AST}} \approx -(\vec{A}_{222}\vec{H})\cdot\vec{\rho}^2. \quad (3)$$

We can see from Eq. (3) that in the presence of misalignments, the magnitude of astigmatism changes linearly with the field, as shown in Fig. 1.

Besides, we can recognize that even in the presence of misalignments, almost no astigmatism exists at the on-axis field point. Therefore, when we achieve an acceptable wavefront at the on-axis field point after the single-field fine-phasing process, we still cannot guarantee the adequate alignment of the system. There can be considerable amounts of astigmatism at the off-axis field point. Therefore, astigmatism is one of the main field-dependent aberrations that needs to be corrected in the multi-field fine-phasing process.

B. Medial Focal Surface

According to NAT, in the presence of misalignments, the medial focal surface can be given by [10]

$$W_{\mathrm{MFS}} = \sum_j W_{220Mj}[(\vec{H} - \vec{\sigma}_j)\cdot(\vec{H} - \vec{\sigma}_j)](\vec{\rho}\cdot\vec{\rho}) = [W_{220M}(\vec{H}\cdot\vec{H}) - 2\vec{A}_{220M}\cdot\vec{H} + B^2_{220M}](\vec{\rho}\cdot\vec{\rho}), \quad (4)$$

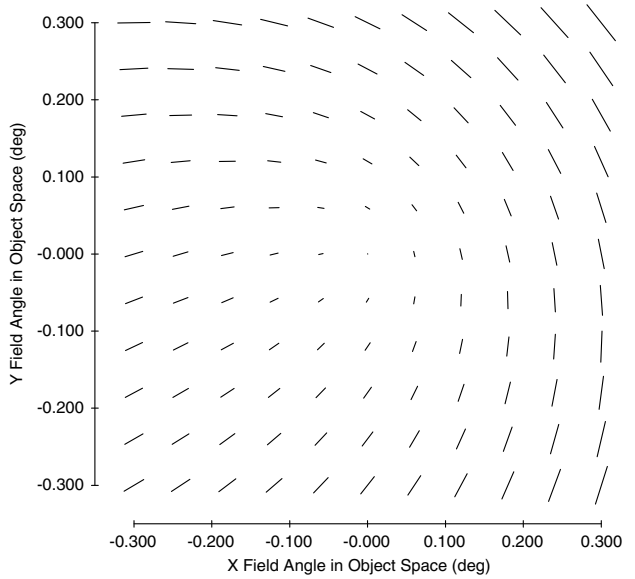

Fig. 1. Full field display (FFD) for the astigmatic aberration field (Z5/Z6, and Zi is the ith Fringe Zernike polynomial) in TMA telescopes with misalignments. We can see that the magnitude of astigmatism is field-dependent.

where W_{220Mj} represents the medial astigmatic component proposed by Hopkins [22],

$$W_{220Mj} = W_{220j} + \frac{1}{2} W_{222j} \tag{5}$$

and $W_{220M} \equiv \sum_j W_{220Mj}$, representing the total aberration contribution for medial focal surface. For TMA telescopes, we can consider $W_{220M} \approx 0$. $\vec{A}_{220M}$ and B^2_{222} are given by

$$\vec{A}_{220M} = \sum_j W_{220Mj}\vec{\sigma}_j, \qquad B^2_{220M} = \sum_j W_{220Mj}\vec{\sigma}_j \cdot \vec{\sigma}_j. \tag{6}$$

For misalignment level perturbations, the magnitude of B^2_{220M} is also proportional to the misalignment squared, and we can consider $B^2_{220M} \approx 0$. Therefore, Eq. (4) can be rewritten as

$$W_{\mathrm{MFS}} \approx (-2\vec{A}_{220M} \cdot \vec{H})(\vec{\rho} \cdot \vec{\rho}). \tag{7}$$

We can see from Eq. (7) that the medial focal surface in TMA telescopes with misalignments is also field-dependent, as shown in Fig. 2.

We should point out that we cannot consider that the magnitude of this term changes linearly with the field, for it is determined by the dot product of two vectors, $\vec{A}_{220M}$ and $\vec{H}$. In other words, it is further affected by the angle between the two vectors.

We can also recognize that even in the presence of misalignments, the medial focus is nearly zero at the on-axis field point. This indicates that when we achieve an acceptable wavefront at the on-axis field point after the single-field fine-phasing process, a large focus can still exist at the off-axis field point. Therefore, the medial focal surface is another dominant field-dependent aberration that needs to be eliminated in the multi-field fine-phasing process.

Besides, we should keep in mind that this kind of field-dependent focus shown in Fig. 2 can not only be induced by mirror misalignments, but also can be induced by the tip–tilt misalignments of the detector. This is one of the important differences between the medial focal surface and other aberrations, such as astigmatism and coma, which are nearly unaffected by the misalignments of the detector. It can be inferred from this fact that the medial focal surface induced by lateral misalignments of different mirrors can be compensated by the tip–tilt of the detector. This will be further discussed in the later parts of this paper.

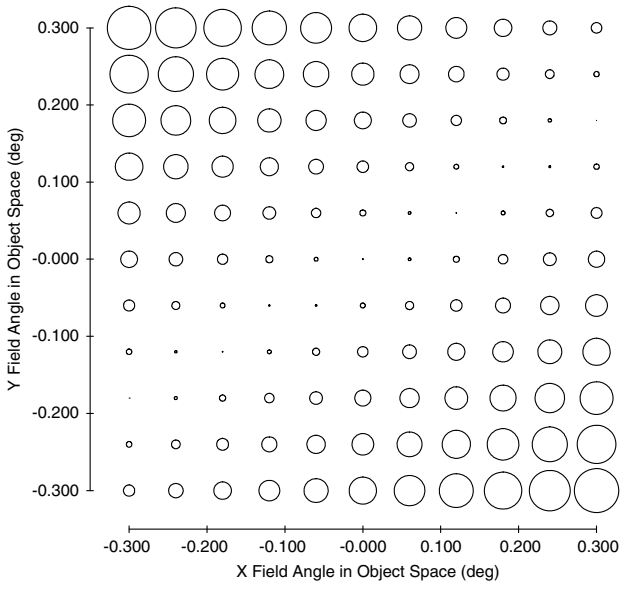

Fig. 2. FFD for the medial focal surface (Z4) in TMA telescopes with misalignments. We can see that the magnitude of the medial focal surface is also field-dependent.

C. Coma Aberration Field

According to NAT, in the presence of misalignments, the coma aberration field can be given by [10,15]

$$\begin{aligned} W_{\mathrm{Coma}} &= \sum_j W_{131j}[(\vec{H} - \vec{\sigma}_j) \cdot \vec{\rho}](\vec{\rho} \cdot \vec{\rho}) \\ &= (W_{131}\vec{H} - \vec{A}_{131}) \cdot \vec{\rho}(\vec{\rho} \cdot \vec{\rho}), \end{aligned} \tag{8}$$

where $W_{131} \equiv \sum_j W_{131j}$, representing the total coma aberration coefficient. $\vec{A}_{131}$ parameterizes the magnitude and the orientation of the net coma field induced by misalignments, which is given by

$$\vec{A}_{131} \equiv \sum_j W_{131j}\vec{\sigma}_j. \tag{9}$$

For TMA telescopes, we can consider that the third-order coma is well corrected in the nominal state, i.e., $W_{131} \approx 0$. Therefore, the coma aberration field in TMA telescopes with misalignments can be rewritten as

$$W_{\mathrm{Coma}} \approx -(\vec{A}_{131} \cdot \vec{\rho})(\vec{\rho} \cdot \vec{\rho}). \tag{10}$$

It can be seen from Eq. (10) that in the presence of misalignments, a considerable field-constant coma will arise over the FOV, as shown in Fig. 3. In other words, when the SM is misaligned, a large coma will typically arise at the center FOV. On the other hand, we should note that after the single-field fine-phasing process, an acceptable wavefront can be established at the on-axis field point. The only possible reason for this is that during the single-field fine-phasing process, the PM is also adjusted to compensate for the on-axis coma due to the misalignments of other mirrors. This is one of the important premises of this work when discussing the alignment strategies for eliminating the field-dependent aberrations in the multi-field fine-phasing process.

3. ANALYTIC STUDY ON THE CURRENT ALIGNMENT STRATEGY FOR ELIMINATING THE FIELD-DEPENDENT ABERRATIONS

The current alignment strategy directly uses the degrees of freedom of the SM, i.e., SM modes, to eliminate the two types of field-dependent aberrations, i.e., astigmatism and medial focal surface. In this section, we will present an analytic study on this alignment strategy. We first analytically investigate the relationships between the field-dependent aberrations and the misalignment parameters, especially the misalignments of the SM. On this basis, we further propose an analytic method for determining the SM moves to eliminate the field-dependent aberration terms. Then, we perform Monte Carlo simulations

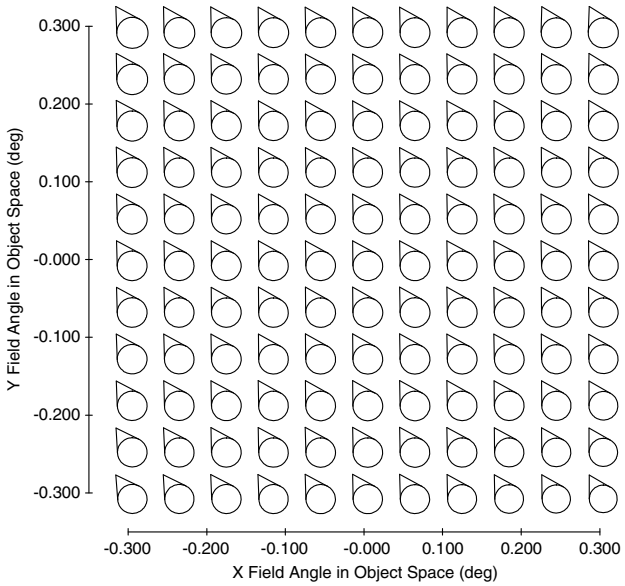

Fig. 3. FFD for the coma aberration field (Z7/Z8) in TMA telescopes with misalignments. We can see that, typically, a large coma aberration will exist at the on-axis field point. The fact that during the single-field fine-phasing process nearly all of the aberrations are well corrected at the on-axis field point indicates that the PM is adjusted to compensate for the coma induced by the misalignments of other mirrors.

to demonstrate the ability of the current strategy to reduce the field dependency of the WFEs.

A. Relationships Between the Field-dependent Aberrations and the Misalignment Parameters

In this part, on one hand, we present a general and qualitative discussion on the relationships between the field-dependent aberrations and the misalignment parameters. On the other hand, we derive the specific expressions of these relationships for TMA telescopes. Meanwhile, some valuable insights into the sensitivities of the field-dependent aberrations to misalignment parameters are provided.

The discussion begins with the relations between the vector that locates the shifted aberration field center for an individual surface, $\vec{\sigma}_j$, and the misalignment parameters of the system. One of the theoretical foundations of NAT is that when an optical surface is misaligned, the aberration behavior of this surface with reference to its local symmetry axis is nearly the same as that in an ordinary symmetric system. The local symmetry axis, which is also called aberration field axis (AFA) in the context of NAT, denotes the line of local symmetry for the field dependence of the aberration field contributions of an individual surface. It is defined by the line that connects the center of curvature and the center of the local entrance pupil. The intersection of the local symmetry axis with the local object plane is called aberration field center. For a perturbed surface, the aberration field center for this surface is usually shifted away from the field center, which is determined by the intersection of the optical axis ray (OAR) with the local object plane.

As shown in Fig. 4, C represents the center of curvature for the nominal spherical surface (in gray), C' represents the center of curvature for the misaligned surface (in black), Q and E are

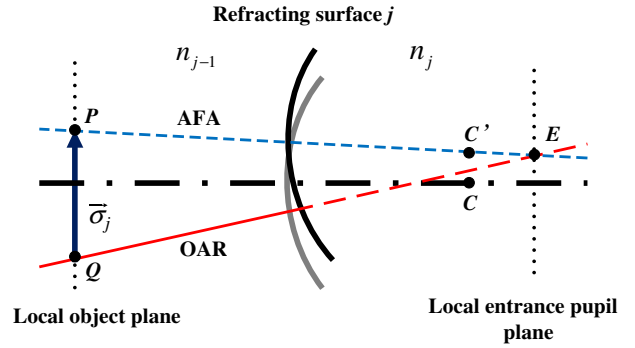

Fig. 4. Schematic representation for vector $\vec{\sigma}_j$ that locates the shifted aberration field center for a perturbed surface with reference to the field center.

the field center and pupil center, respectively. P is the aberration field center for this surface. In NAT, we use the vector $\vec{\sigma}_j$ to locate the position of the aberration field center, P, with reference to the field center, Q.

We can see from Fig. 4 that the vector $\vec{\sigma}_j$ is determined by the positions of three points, Q, E, and C'. The position of C' is associated with the misalignment parameters of this surface, and the positions of P and Q are associated with the misalignment parameters of the preceding surfaces [23]. Consequently, the vector $\vec{\sigma}_j$ is determined by the misalignments of surface j and those surfaces located before this surface. Specifically, the vector $\vec{\sigma}_j$ can be expressed as a linear combination of the misalignments of surface j and the preceding surfaces,

$$\vec{\sigma}_j = \sum_{i=1}^{j} (s_{ji}\vec{V}_i + t_{ji}\vec{\beta}_i), \tag{11}$$

where i is the surface index, $\vec{V}$ and $\vec{\beta}$ are the vectors representing the magnitude and orientation of the individual surface decenter and tip–tilt parameters, respectively. They are given by

$$\vec{V} \equiv \begin{bmatrix} XDE \\ YDE \end{bmatrix}, \qquad \vec{\beta} \equiv \begin{bmatrix} -BDE \\ ADE \end{bmatrix}, \tag{12}$$

where XDE and YDE are the surface vertex decenters in the $x-z$ and $y-z$ plane, respectively, and BDE and ADE are the surface tip-tilts in the $x-z$ and $y-z$ plane, respectively. s and t represent the corresponding coefficients.

On the other hand, we can see from Section 2 that the magnitude and orientation of the two field-dependent aberrations induced by misalignments are directly related to two vectors, i.e., $\vec{A}_{222}$ and $\vec{A}_{220M}$. Both of these vectors can be expressed as a combination of the vectors locating the shifted aberration field center for each individual surface, each weighted by the aberration coefficient for the corresponding surface. Here, we use a generalized formula to express them,

$$\vec{A}_{klm} = \sum_j W_{klmj}\vec{\sigma}_j, \tag{13}$$

where W_{klmj} represents a certain type of aberration coefficient for surface j. Specifically, here, W_{klmj} can represent W_{222j} or W_{220Mj}. Then, by substituting Eq. (11) into Eq. (13), we can obtain

$$\vec{A}_{klm} = \sum_i (S_i^{(klm)} \vec{V}_i + T_i^{(klm)} \vec{\beta}_i), \tag{14}$$

where

$$S_i^{(klm)} = \sum_{j=i} W_{klmj} s_{ji}, \qquad T_i^{(klm)} = \sum_{j=i} W_{klmj} t_{ji}. \tag{15}$$

Substituting Eqs. (14) and (15) into Eqs. (3) and (5), respectively, we can obtain the expressions of the two field-dependent aberrations in terms of the misalignment parameters of the system, which are given by

$$W_{\mathrm{AST}} \approx -\left[\sum_i (S_i^{(222)} \vec{V}_i + T_i^{(222)} \vec{\beta}_i) \vec{H}\right] \cdot \vec{\rho}^2, \tag{16}$$

$$W_{\mathrm{MS}} \approx -2\left[\sum_i (S_i^{(220M)} \vec{V}_i + T_i^{(220M)} \vec{\beta}_i) \cdot \vec{H}\right] (\vec{\rho} \cdot \vec{\rho}). \tag{17}$$

Equations (14)–(17) can provide some valuable insights into the sensitivities of the field-dependent aberrations to the misalignments of the system. We can see that the two field-dependent aberrations induced by misalignments consist of a strong linear function of the misalignment parameters of the system. This indicates that the sensitivity of the field-dependent aberrations to one misalignment parameter is unaffected by the misalignment parameters of the other surfaces. On the other hand, by examining Eq. (15), we can recognize that this sensitivity is not only associated with the corresponding aberration coefficients of this surface, but also is tightly associated with the aberration coefficients of the subsequent surfaces (but has nothing to do with the aberration coefficients of the preceding surfaces).

Then, we begin to derive the specific expressions of S_i^{klm} and T_i^{klm} for TMA telescopes. Here, we choose the tertiary mirror (TM) as the reference and assume that the PM and SM are misaligned relative to the TM. The relationships between the shifted aberration field center for each individual surface and the misalignment parameters can be given by [21,23]

$$\vec{\sigma}_{\mathrm{PM}}^{\mathrm{sph}} = \frac{1}{\bar{u}_{\mathrm{PM}}} \vec{\beta}_{\mathrm{PM}}, \tag{18}$$

$$\vec{\sigma}_{\mathrm{SM}}^{\mathrm{sph}} = \frac{2}{\bar{u}_{\mathrm{PM}}} \vec{\beta}_{\mathrm{PM}} + \frac{1}{\bar{u}_{\mathrm{PM}}(d_1 + r_{\mathrm{SM}})} (\vec{V}_{\mathrm{PM}} - \vec{V}_{\mathrm{SM}} - r_{\mathrm{SM}} \vec{\beta}_{\mathrm{SM}}), \tag{19}$$

$$\vec{\sigma}_{\mathrm{TM}}^{\mathrm{sph}} = \frac{2}{\bar{u}_{\mathrm{PM}}} \vec{\beta}_{\mathrm{PM}} + \frac{(2d_2 - r_{\mathrm{SM}} + 2r_{\mathrm{TM}}) \vec{V}_{\mathrm{PM}} - (2d_2 + 2r_{\mathrm{TM}})(\vec{V}_{\mathrm{SM}} + r_{\mathrm{SM}} \vec{\beta}_{\mathrm{SM}})}{\bar{u}_{\mathrm{PM}}(2d_1 d_2 - d_1 r_{\mathrm{SM}} + d_2 r_{\mathrm{SM}} + 2d_1 r_{\mathrm{TM}} + r_{\mathrm{SM}} r_{\mathrm{TM}})}, \tag{20}$$

$$\vec{\sigma}_{\mathrm{PM}}^{\mathrm{asph}} = \vec{0}, \tag{21}$$

$$\vec{\sigma}_{\mathrm{SM}}^{\mathrm{asph}} = \frac{1}{d_1 \bar{u}_{\mathrm{PM}}} (\vec{V}_{\mathrm{PM}} - \vec{V}_{\mathrm{SM}} + 2d_1 \vec{\beta}_{\mathrm{PM}}), \tag{22}$$

$$\vec{\sigma}_{\mathrm{TM}}^{\mathrm{asph}} = \frac{2}{\bar{u}_{\mathrm{PM}}} \vec{\beta}_{\mathrm{PM}} + \frac{(2d_2 - r_{\mathrm{SM}}) \vec{V}_{\mathrm{PM}} - 2d_2 (\vec{V}_{\mathrm{SM}} + r_{\mathrm{SM}} \vec{\beta}_{\mathrm{SM}})}{\bar{u}_{\mathrm{PM}}(2d_1 d_2 - d_1 r_{\mathrm{SM}} + d_2 r_{\mathrm{SM}})}, \tag{23}$$

where $\bar{u}_{\mathrm{PM}}$ corresponds to the paraxial chief ray angle at the PM, d_1 is the distance from the PM to SM, d_2 is the distance from the SM to TM, r_{SM} and r_{TM} corresponds to the radius of the SM and TM, respectively, and the up-script sph and asph indicate that the field center displacement vectors are associated with the spherical base curve and the aspheric departure from the spherical base curve of each individual surface, respectively.

For TMA telescopes, the two vectors that determine the magnitude and orientation of the two field-dependent aberrations, $\vec{A}_{222}$ and $\vec{A}_{220M}$, can be expressed as

$$\vec{A}_{222} = S_{\mathrm{PM}}^{(222)} \vec{V}_{\mathrm{PM}} + T_{\mathrm{PM}}^{(222)} \vec{\beta}_{\mathrm{PM}} + S_{\mathrm{SM}}^{(222)} \vec{V}_{\mathrm{SM}} + T_{\mathrm{SM}}^{(222)} \vec{\beta}_{\mathrm{SM}}, \tag{24}$$

$$\vec{A}_{220M} = S_{\mathrm{PM}}^{(220M)} \vec{V}_{\mathrm{PM}} + T_{\mathrm{PM}}^{(220M)} \vec{\beta}_{\mathrm{PM}} + S_{\mathrm{SM}}^{(220M)} \vec{V}_{\mathrm{SM}} + T_{\mathrm{SM}}^{(220M)} \vec{\beta}_{\mathrm{SM}}, \tag{25}$$

where

$$\begin{aligned} S_{\mathrm{PM}}^{(222)} &= \frac{1}{\bar{u}_{\mathrm{PM}}(d_1 + r_{\mathrm{SM}})} W_{222,\mathrm{SM}}^{\mathrm{sph}} + \frac{1}{d_1 \bar{u}_{\mathrm{PM}}} W_{222,\mathrm{SM}}^{\mathrm{asph}} \\ &+ \frac{(2d_2 - r_{\mathrm{SM}} + 2r_{\mathrm{TM}})}{\bar{u}_{\mathrm{PM}}(2d_1 d_2 - d_1 r_{\mathrm{SM}} + d_2 r_{\mathrm{SM}} + 2d_1 r_{\mathrm{TM}} + r_{\mathrm{SM}} r_{\mathrm{TM}})} W_{222,\mathrm{TM}}^{\mathrm{sph}} \\ &+ \frac{(2d_2 - r_{\mathrm{SM}})}{\bar{u}_{\mathrm{PM}}(2d_1 d_2 - d_1 r_{\mathrm{SM}} + d_2 r_{\mathrm{SM}})} W_{222,\mathrm{TM}}^{\mathrm{asph}}, \end{aligned} \tag{26}$$

$$T_{\mathrm{PM}}^{(222)} = \frac{1}{\bar{u}_{\mathrm{PM}}} W_{222,\mathrm{PM}}^{\mathrm{sph}} + \frac{2}{\bar{u}_{\mathrm{PM}}} (W_{222,\mathrm{SM}}^{\mathrm{sph}} + W_{222,\mathrm{SM}}^{\mathrm{asph}} + W_{222,\mathrm{TM}}^{\mathrm{sph}} + W_{222,\mathrm{TM}}^{\mathrm{asph}}), \tag{27}$$

$$\begin{aligned} S_{\mathrm{SM}}^{(222)} &= \frac{-1}{\bar{u}_{\mathrm{PM}}(d_1 + r_{\mathrm{SM}})} W_{222,\mathrm{SM}}^{\mathrm{sph}} + \frac{-1}{d_1 \bar{u}_{\mathrm{PM}}} W_{222,\mathrm{SM}}^{\mathrm{asph}} \\ &+ \frac{-(2d_2 + 2r_{\mathrm{TM}})}{\bar{u}_{\mathrm{PM}}(2d_1 d_2 - d_1 r_{\mathrm{SM}} + d_2 r_{\mathrm{SM}} + 2d_1 r_{\mathrm{TM}} + r_{\mathrm{SM}} r_{\mathrm{TM}})} W_{222,\mathrm{TM}}^{\mathrm{sph}} \\ &+ \frac{-2d_2}{\bar{u}_{\mathrm{PM}}(2d_1 d_2 - d_1 r_{\mathrm{SM}} + d_2 r_{\mathrm{SM}})} W_{222,\mathrm{TM}}^{\mathrm{asph}}, \end{aligned} \tag{28}$$

$$\begin{aligned} T_{\mathrm{SM}}^{(222)} &= \frac{-r_{\mathrm{SM}}}{\bar{u}_{\mathrm{PM}}(d_1 + r_{\mathrm{SM}})} W_{222,\mathrm{SM}}^{\mathrm{sph}} \\ &+ \frac{-(2d_2 + 2r_{\mathrm{TM}}) r_{\mathrm{SM}}}{\bar{u}_{\mathrm{PM}}(2d_1 d_2 - d_1 r_{\mathrm{SM}} + d_2 r_{\mathrm{SM}} + 2d_1 r_{\mathrm{TM}} + r_{\mathrm{SM}} r_{\mathrm{TM}})} W_{222,\mathrm{TM}}^{\mathrm{sph}} \\ &+ \frac{-2d_2 r_{\mathrm{SM}}}{\bar{u}_{\mathrm{PM}}(2d_1 d_2 - d_1 r_{\mathrm{SM}} + d_2 r_{\mathrm{SM}})} W_{222,\mathrm{TM}}^{\mathrm{asph}}. \end{aligned} \tag{29}$$

By replacing the astigmatic aberration coefficient for each individual surface with the corresponding aberration coefficient for the medial focal surface in $S_{\mathrm{PM}}^{(222)}$, $T_{\mathrm{PM}}^{(222)}$, $S_{\mathrm{SM}}^{(222)}$, and $T_{\mathrm{SM}}^{(222)}$,

we can also obtain the specific expressions for $S_{\mathrm{PM}}^{(220M)}$, $T_{\mathrm{PM}}^{(220M)}$, $S_{\mathrm{SM}}^{(220M)}$, and $T_{\mathrm{SM}}^{(220M)}$.

Equations (24)–(29) further illustrate those representations presented below Eq. (17). The sensitivity of the two field-dependent aberrations to one misalignment parameter of the system is nearly unaffected by the misalignments of other surfaces, but it is tightly associated with the aberration coefficients of the other surfaces (the subsequent surfaces). Besides, the fact that the magnitude of the field-dependent aberrations corresponds linearly to the misalignment parameters of the PM and SM, also presents the possibility of compensating the effects of the misalignments of one mirror with the misalignments of the others. This is the theoretical basis for us to use SM moves to eliminate the field-dependent aberrations that may be induced by the misalignments of other mirrors.

B. Analytic Method for Determining the Corrective SM Moves to Eliminate the Field-Dependent Aberrations

In this part, we first discuss how to quantify the magnitude and orientation of the two vectors, $\vec{A}_{222}$ and $\vec{A}_{220M}$, using wavefront measurements at several field points. Then, we continue to determine the corrective SM moves for minimizing the magnitude of these two vectors and, thus, eliminating the field-dependent aberrations. Meanwhile, we will explicitly point out the minimum number of wavefront measurements that are needed for us to accomplish this work.

According to NAT, the net astigmatic aberration field induced by misalignments can be expressed as

$$\Delta W_{\mathrm{AST}} = (-\vec{A}_{222}\vec{H} + \frac{1}{2}\vec{B}_{222}^{2}) \cdot \vec{\rho}^{2}, \tag{30}$$

where Δ is the difference operator, and ΔW_{AST} represents the difference between the astigmatism in the presence of misalignments and that in the nominal state, i.e., the net astigmatic aberration contribution induced by misalignments.

Using the vector multiplication of NAT, Eq. (30) can be rewritten as

$$\Delta W_{\mathrm{AST}} = \begin{bmatrix} -\vec{A}_{222,x}H_x + \vec{A}_{222,y}H_y + \frac{1}{2}\vec{B}_{222,x}^{2} \\ -\vec{A}_{222,y}H_x - \vec{A}_{222,x}H_y + \frac{1}{2}\vec{B}_{222,y}^{2} \end{bmatrix} \cdot \begin{bmatrix} \rho^2\cos(2\phi) \\ \rho^2\sin(2\phi) \end{bmatrix}, \tag{31}$$

where the subscripts x, y represent the two components of a vector. Here, the x axis is used as the reference axis, and ϕ is measured counter-clockwise from it in order to be in accord with the tradition of optical testing.

Since wavefront measurements typically provide the Zernike polynomial coefficients to the wavefront, the correspondence between the Seidel and Zernike coefficients can be utilized to compute the unknowns. Though the exact correspondence between the Seidel coefficients and Zernike polynomials is generally an infinite sum, as discussed in detail by Tyson in Ref. [24], in our paper, only the first 16 items of Fringe Zernike coefficients are considered. The higher-order Zernike coefficients that are fitted against the wavefront are reasonably small, so they can be ignored. According to this correspondence, referring to Eq. (31), we obtain

$$\begin{bmatrix} -H_x & H_y & \frac{1}{2} & 0 \\ -H_y & -H_x & 0 & \frac{1}{2} \end{bmatrix} \begin{bmatrix} \vec{A}_{222,x} \\ \vec{A}_{222,y} \\ \vec{B}_{222,x}^{2} \\ \vec{B}_{222,y}^{2} \end{bmatrix} = \Delta \begin{bmatrix} C_5 - 3C_{12} \\ C_6 - 3C_{13} \end{bmatrix}, \tag{32}$$

where C_i is the ith Fringe Zernike coefficient for representing the WFE. We can see that there are four unknowns: $\vec{A}_{222,x}$, $\vec{A}_{222,y}$, $\vec{B}_{222,x}^{2}$, and $\vec{B}_{222,y}^{2}$. In order to solve them, wavefront measurements at a minimum of two off-axis field points are sufficient. If wavefront measurements at more than two field points are available, the four unknowns can be obtained by solving the least-square solutions of the over-determined equations.

Then, we continue to quantify $\vec{A}_{220M}$. According to NAT, the net medial focal surface induced by misalignments can be expressed as

$$\Delta W_{\mathrm{MFS}} = (-2\vec{A}_{220M} \cdot \vec{H} + B_{220M}^{2})(\vec{\rho} \cdot \vec{\rho}). \tag{33}$$

Using the vector multiplication of NAT, Eq. (33) can be rewritten as

$$\Delta W_{\mathrm{MFS}} = (-2A_{220M,x}H_x - 2A_{220M,y}H_y + B_{220M}^{2})(\vec{\rho} \cdot \vec{\rho}). \tag{34}$$

According to the relationship between the Seidel coefficients and the Zernike coefficients, we can obtain

$$\begin{bmatrix} -1 & -1 & \frac{1}{2} \end{bmatrix} \begin{bmatrix} A_{220M,x} \\ A_{220M,y} \\ B_{220M}^{2} \end{bmatrix} = \frac{1}{2}\Delta(2C_4 - 6C_9 + 12C_{16}). \tag{35}$$

We can see that there are three unknows: $A_{220M,x}$, $A_{220M,y}$, and B_{220M}^{2}. In order to solve them, wavefront measurements at a minimum of three field points are needed, for wavefront measurements at one field point only provide one equation for the medial focal surface. If wavefront measurements at more than three field points are available, the three unknowns can be obtained by solving the least-square solutions of the over-determined equations.

After quantifying the two vectors that determine the magnitude and orientation of the two types of field-dependent aberrations, $\vec{A}_{222}$ and $\vec{A}_{220M}$, we begin to determine the corrective SM moves to minimize them.

Supposing $\Delta\vec{V}_{\mathrm{SM}} \equiv \begin{bmatrix} \Delta XDE_{\mathrm{SM}} \\ \Delta YDE_{\mathrm{SM}} \end{bmatrix}$ and $\Delta\vec{\beta}_{\mathrm{SM}} \equiv \begin{bmatrix} -\Delta BDE_{\mathrm{SM}} \\ \Delta ADE_{\mathrm{SM}} \end{bmatrix}$ are the corrective SM moves used to minimize $\vec{A}_{222}$ and $\vec{A}_{220M}$, we can have

$$-\vec{A}_{222} = S_{\mathrm{SM}}^{(222)}\Delta\vec{V}_{\mathrm{SM}} + T_{\mathrm{SM}}^{(222)}\Delta\vec{\beta}_{\mathrm{SM}}, \tag{36}$$

$$-\vec{A}_{220M} = S_{\mathrm{SM}}^{(220M)}\Delta\vec{V}_{\mathrm{SM}} + T_{\mathrm{SM}}^{(220M)}\Delta\vec{\beta}_{\mathrm{SM}}. \tag{37}$$

Since $\vec{A}_{222}$ and $\vec{A}_{220M}$ can be quantified with wavefront measurements at several field points, using Eqs. (36) and (37), we can determine the corrective SM moves used to minimize $\vec{A}_{222}$ and $\vec{A}_{220M}$ thus eliminating the two types of field-dependent aberrations.

C. Simulations

To demonstrate the ability of the current alignment strategy with our analytic method to reduce the field dependency of the WFEs, relevant simulations will be conducted in this part. First, for a randomly selected case, we will show the full field displays (FFDs) of the two field-dependent aberrations before and after applying the computed corrective SM moves to the system. Then, Monte Carlo simulations will further be conducted to compare the field dependency of the WFEs before and after correction. The results show that the current strategy can greatly minimize the field dependency of the WFEs.

A TMA telescope with similar optical parameters with a JWST will be used in the simulations. The optical layout of this telescope and its optical prescription, third-order aberration coefficients, which are needed in the simulations, are presented in Appendix A. As presented in the previous part, wavefront measurements at a minimum of three arbitrary field points can be used to compute the corrective SM moves. In this part, we utilize wavefront measurements at four field points, i.e., (−0.1°, 0.1°), (0.1°,0.1°), (−0.1°, −0.1°), and (−0.1°, 0.1°), to determine the corrective SM moves for eliminating the field-dependent aberrations.

We first artificially introduce a set of misalignments of the PM and SM into the simulation software Code V. The resulting wavefronts at the four field points can be obtained from simulation software. Utilizing the analytic computation approach presented in this paper, the corrective SM moves can be obtained. The specific misalignments of the PM and SM simulated here are presented in row A and row B of Table 1, respectively. In this case, the on-axis coma is nearly in a compensated state ($C7 = 0.0032$, $C8 = 0.0366$). The misalignments of the SM after correction are presented in row C of Table 1.

The FFDs for the medial focal surface and astigmatism before and after correction are shown in Fig. 5. We can see that the two types of field-dependent aberrations are both eliminated.

To further demonstrate the ability of the current alignment strategy with our analytic method to reduce the field dependency of the WFEs, we will perform Monte Carlo simulations and make a comparison between the magnitudes of the two types of the field-dependent aberrations before and after the correction. We can see from Eqs. (3) and (7) that the vectors $\vec{A}_{222}$ and $\vec{A}_{220M}$ determine the field dependencies of the two field-dependent aberrations, respectively. Therefore, here, we use the magnitudes of these two vectors, $|A_{222}|$ and $|A_{220M}|$, to represent the magnitudes of the field dependencies of the two field-dependent aberrations, i.e., astigmatism and medial focal surface, respectively (the correspondence between the Seidel coefficients and the Fringe Zernike coefficients have been considered).

Table 1. Introduced PM and SM Misalignments (A and B) and the SM Misalignments After Correction (C)

	XDE (mm)	*YDE* (mm)	*ADE* (deg)	*BDE* (deg)
A	0.1113	−0.0996	0.0010	−0.0004
B	−0.0283	−0.1410	0.0060	0.0045
C	−0.0011	−0.1486	0.0012	0.0000

On one hand, we first select 100 misalignment states, which meet the premise for the aberration condition of the JWST-like space telescopes before the multi-field fine-phasing process, i.e., the PM and SM are in a compensated state for an on-axis coma. Specifically, for the perturbation range of $XDE, YDE \in [-0.2\text{ mm}, 0.2\text{ mm}]$, and $ADE, BDE \in [-0.005°, 0.005°]$, we introduce tremendous amounts of misalignment states into the optical simulation software and select 100 states that are in a nearly compensated state for the on-axis coma. For these 100 misalignment states, the magnitudes of the field dependencies of the two field-dependent aberrations before and after applying the computed corrective SM moves to the system are shown in Fig. 6. It can be seen that the field dependencies of the two field-dependent aberrations are greatly reduced.

To present a more overall understanding of the ability of the current alignment strategy with our analytic method to reduce the field dependency of the WFEs, three different cases with different misalignment ranges will be further considered in the Monte Carlo simulations. The specific misalignment ranges in each case are presented in Table 2. For each case, 200 misalignment states will be generated with similar methods to meet the premise that the PM and SM are in a compensated state for the on-axis coma. For each misalignment state, we compute the field dependencies of the two field-dependent aberrations (represented by $|A_{222}|$ and $|A_{220M}|$, respectively) before and after applying the corrective SM moves into the system. The mean values of the field dependencies of the two field-dependent aberrations for the 200 misalignment states in each case before and after correction are shown in Table 3.

It can be seen from Table 3 that in all three cases the field dependencies of the two types of the field-dependent aberrations can be greatly decreased. Therefore, the current strategy can minimize the field-dependency of the WFEs using our analytic method for determining the corrective SM moves.

4. NEW ALIGNMENT STRATEGY FOR ELIMINATING THE FIELD-DEPENDENT ABERRATIONS

In this section, we first reveal a deep-rooted problem that exists in the current alignment strategy for eliminating the field-dependent aberrations, which can decrease the alignment efficiency of the multi-field fine-phasing process. Based on a deep understanding of the aberration condition before the multi-field fine-phasing process and the reason for the low efficiency of the current alignment strategy, we propose a new alignment strategy. Then, we perform detailed simulations and some additional discussions to demonstrate the alignment efficiency and rationality of this new strategy. Lastly, we further illustrate the problem of the current alignment strategy for the case of a tip-tilted detector, which, on the other hand, can also further demonstrate the rationality of the new alignment strategy.

A. Problem of the Current Alignment Strategy

Before revealing the problem of the current alignment strategy, we first emphasize the true meaning of "eliminating the field-dependent aberrations." During the single-field fine-phasing

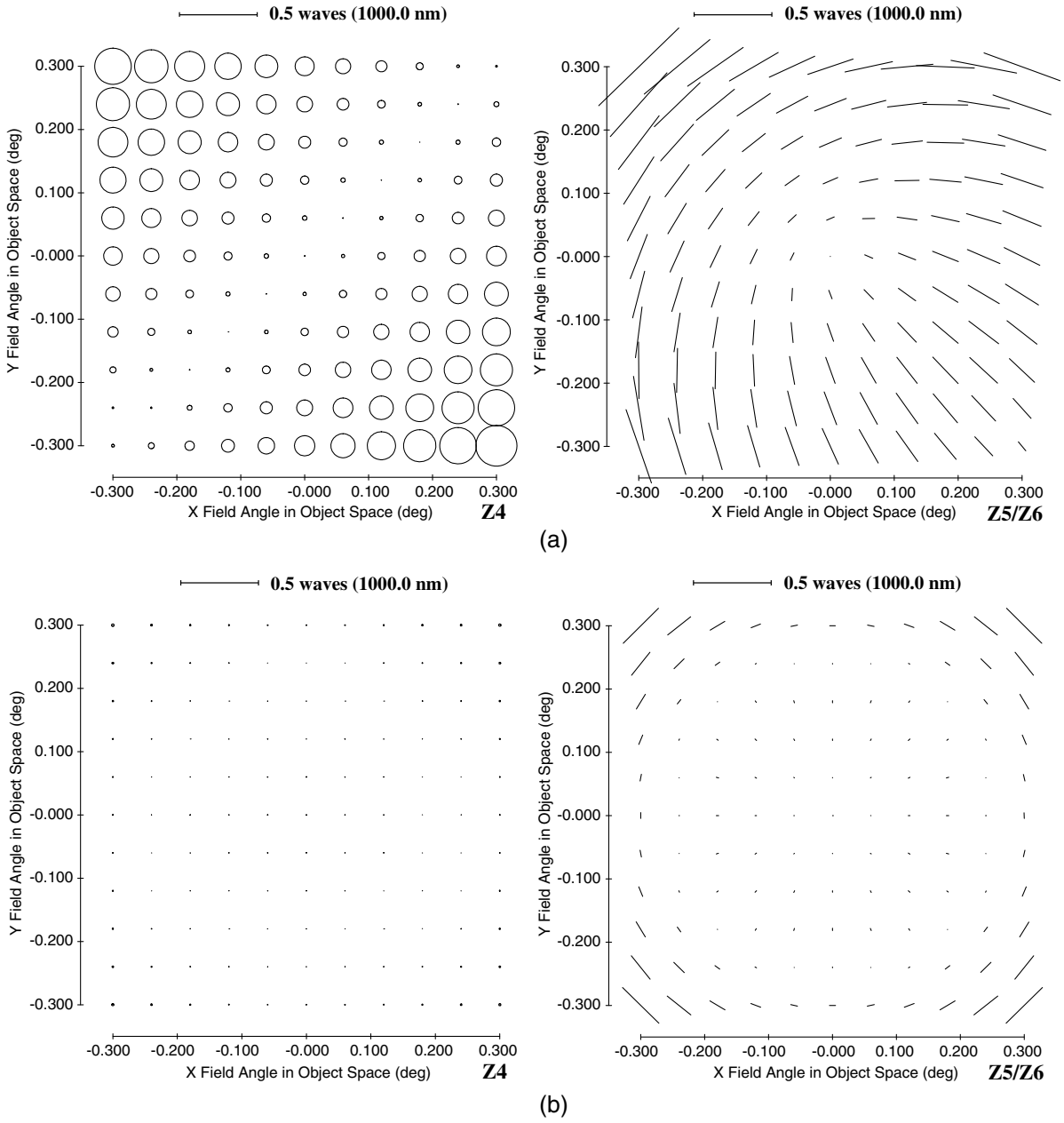

Fig. 5. FFDs of the medial focal surface (Z4) and astigmatism (Z5/Z6) (a) before and (b) after correction for the misalignment state specified above. We can see that these two types of field-dependent aberrations are both well corrected.

process, we have established an acceptable wavefront at the on-axis field point. However, interrogating off-axis field points can reveal a large WFE, which indicates the presence of some field-dependent aberrations. We need to further correct these field-dependent aberrations to obtain an acceptable wavefront over the whole FOV. More importantly, here, there is an underlying meaning of "eliminating the field-dependent aberrations", i.e., the wavefront at the on-axis field point should be maintained after eliminating the field-dependent aberrations.

While the current strategy can greatly reduce the field dependency of the WFEs, however, when using the SM modes to correct both types of field-dependent aberrations, the WFE at the on-axis field point, which is usually dominated by a coma, cannot be controlled at the same time. Consequently, a large field-constant coma can be introduced into the system in this process. For the set of misalignments of PM and SM presented in Table 1, the coma aberration field before and after applying the corrective SM moves to eliminate the field-dependent aberrations is shown in Fig. 7. We can see that, while the two types of field-dependent aberrations are well corrected, as shown in Fig. 5, a large field-constant coma is introduced into the system.

To further illustrate this problem, the magnitudes of the coma aberration at the on-axis field point before and after correction for the 100 misalignment states simulated in the third part (Part C) of Section 3 are shown in Fig. 8. Here, we use

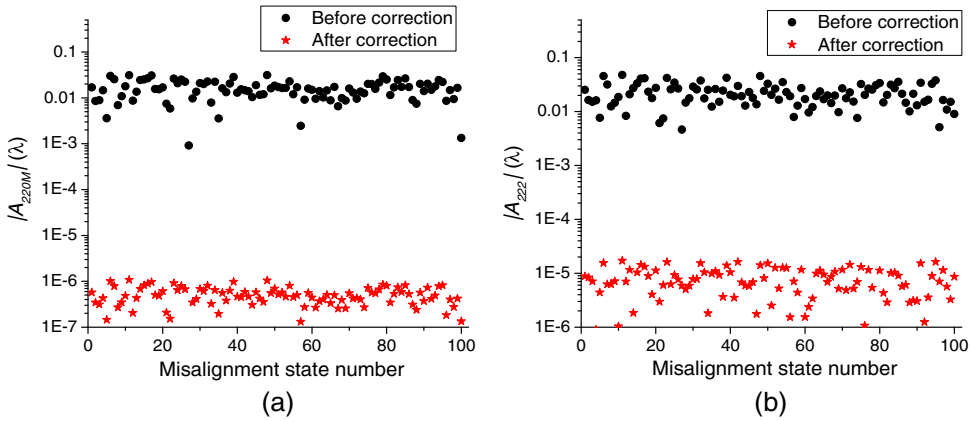

Fig. 6. Magnitudes of the field dependencies of (a) the medial focal surface and (b) astigmatism before and after applying the corrective SM moves to the system. $|A_{220M}|$ and $|A_{222}|$ are measured in $\lambda(\lambda = 1000.0$ nm), and they are computed with a normalized field height of 0.1°.

Table 2. Misalignment Ranges of the Three Different Cases Considered in the Monte Carlo Simulations

	XDE,*YDE* (mm)	*ADE*,*BDE* (deg)
Case 1	[−0.1,0.1]	[−0.002,0.002]
Case 2	[−0.2,0.2]	[−0.005,0.005]
Case 3	[−0.5,0.5]	[−0.01,0.01]

Table 3. Mean Magnitudes of the Field Dependencies of the Two Types of Field-Dependent Aberrations Before and After Correction (Represented by A and B, Respectively) in the Three Cases[a]

	$\lvert A_{220M}\rvert$		$\lvert A_{222}\rvert$	
	A	B	A	B
Case 1	1.1×10^{-2}	3.4×10^{-7}	1.5×10^{-2}	4.4×10^{-6}
Case 2	4.8×10^{-2}	1.6×10^{-6}	7.1×10^{-2}	2.7×10^{-5}
Case 3	6.0×10^{-2}	2.8×10^{-6}	9.7×10^{-2}	4.0×10^{-5}

[a]$|A_{220M}|$ and $|A_{222}|$ are measured in λ ($\lambda = 1000$ nm), and they are computed with a normalized field height of 0.1°.

$|C_{\mathrm{COMA}}|$ ($|C_{\mathrm{COMA}}| \equiv \sqrt{C_7^2 + C_8^2}$, and C_i is the ith Fringe Zernike coefficient) to represent the magnitude of the coma aberration. We can see that the on-axis coma is nearly in a compensated state before correction, and a large on-axis coma will be introduced into the system after correction.

Therefore, in practice, once the SM corrections are applied, the PM must be adjusted to reestablish an acceptable WFE on axis [4], which, unfortunately, can further introduce some field-dependent aberrations. This indicates that the process of eliminating the field-dependent aberrations with the current alignment strategy is essentially an iterative alignment process of the PM segments and SM, which is clearly shown in Fig. 1 of Ref. [6]. While after enough times of iterative alignment, an acceptable WFE over the whole FOV can be obtained, we should recognize that the alignment efficiency is low.

One of the most important reasons for this low efficiency is that the field-dependent and the field-constant aberrations cannot be corrected at the same time. After eliminating the field-dependent aberrations using SM modes, a large field-constant coma will arise. After adjusting the PM to reestablish an acceptable WFE on axis, the field-dependent aberrations will further be reintroduced into the system, because when correcting the on-axis coma by adjusting the PM, only the aberrations at the on-axis point are concerned, and the field-dependent aberrations cannot be controlled at the same time. We can infer that quite a lot of iterations may be needed to achieve the adequate alignment of the system.

We should note that adjusting the PM segments to achieve an acceptable wavefront on axis after moving the SM is really a complicated and time-consuming work. To this end, we need go back to the global alignment commissioning step and then repeat the coarse-phasing and single-field fine-phasing process. Therefore, we can conclude that the efficiency of the current alignment strategy is low.

In this paper, the current alignment strategy mainly refers to the one presented in Refs. [4,7]. In effect, there exists another strategy for eliminating the field-dependent aberrations, which is presented in Ref. [25]. Specifically, in this strategy, the SM is adjusted to achieve a least-square alignment state of the system in the multi-field fine-phasing process. Note that the field-dependent and field-constant aberrations cannot be corrected simultaneously just by adjusting the SM. We can infer that after using this strategy a field-constant coma will also be introduced into the system, but the magnitude of it is relatively small; the magnitudes of the two field-dependent aberrations will be reduced, but cannot be eliminated. This is what "least-square alignment state" means in this case. Therefore, after adjusting the SM using this strategy, we also need to adjust the PM to reestablish an acceptable wavefront on axis; since the field-dependent aberrations have not been eliminated by adjusting the SM (and some may also be reintroduced into the system after adjusting the PM), the SM will be further readjusted to achieve a least-square state of the system [25]. We can easily recognize that this strategy also needs iterative alignment of the PM and the SM before the system is completely aligned.

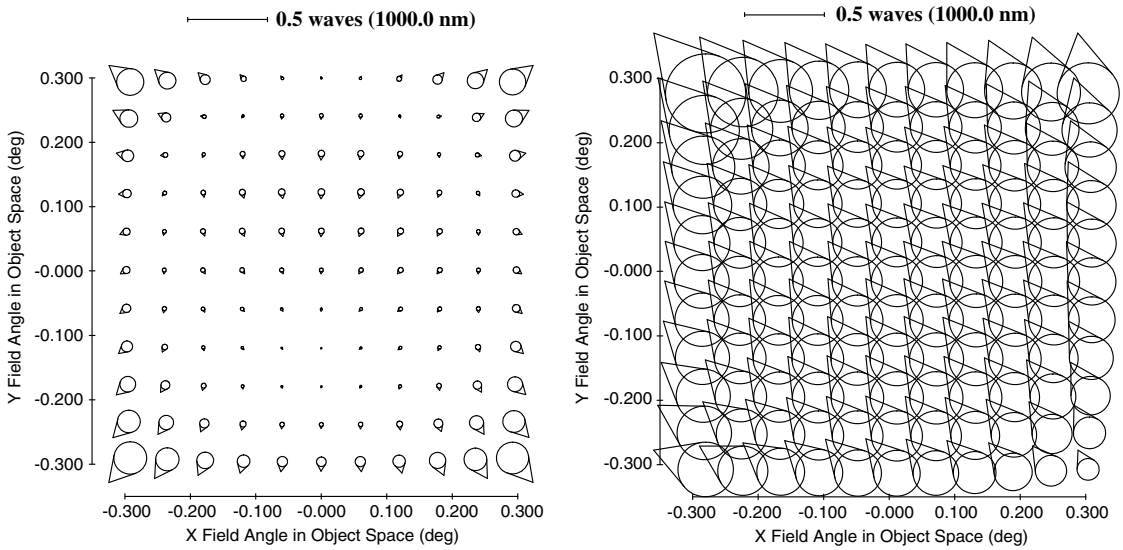

Fig. 7. FFDs for the coma (Z7/Z8) (a) before and (b) after applying the corrective SM moves to eliminate the field-dependent aberrations. We can see that the on-axis coma is nearly in a compensated state before correction, and a large coma is introduced into the system after correction.

Therefore, while the two existing strategies seem different, they have the same deep-rooted problems, i.e., the field-dependent and field-constant aberrations cannot be eliminated simultaneously, and the iterative alignment of the PM and SM are usually needed.

B. New Alignment Strategy for Eliminating the Field-dependent Aberrations

To improve the alignment efficiency of the multi-field fine-phasing process, we propose here a new alignment strategy. In this new strategy, we do not directly use the SM degrees of freedom to eliminate both types of the field-dependent aberrations. On one hand, we adjust the SM to eliminate the astigmatism, while maintaining an acceptable WFE on axis. This can be interpreted as eliminating the astigmatism by rotating the SM around its coma pivot point. Then, the residual medial focal surface can easily be corrected by slightly adjusting the detector. One of the main characteristics of this new strategy is that when correcting one aberration, those aberrations that have been corrected will not be further reintroduced into the system. Specifically, when using the SM modes to correct the field-dependent astigmatism, the on-axis coma can also be controlled at the same time; when using the detector to correct the residual medial focal surface, other aberrations are unaffected. Consequently, we can infer that one of the main advantages of this strategy is that the PM is no longer needed to readjust in the multi-field fine-phasing process, and, therefore, greatly improves the alignment efficiency of the multi-field fine-phasing process.

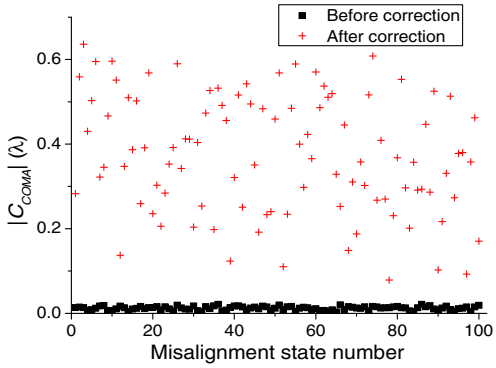

Fig. 8. Magnitudes of the on-axis coma before and after applying the SM moves to correct the field-dependent aberrations. We can see that a large on-axis coma will arise after correction.

Here, we first determine the corrective SM modes to eliminate the astigmatism, while assuring that no field-constant coma will be introduced into the system, which can be expressed as

$$-\vec{A}_{222} = S_{\mathrm{SM}}^{(222)}\Delta\vec{V}_{\mathrm{SM}} + T_{\mathrm{SM}}^{(222)}\Delta\vec{\beta}_{\mathrm{SM}}, \tag{38}$$

$$0 = S_{\mathrm{SM}}^{(131)}\Delta\vec{V}_{\mathrm{SM}} + T_{\mathrm{SM}}^{(131)}\Delta\vec{\beta}_{\mathrm{SM}}. \tag{39}$$

Here, $S_{\mathrm{SM}}^{(131)}$ and $T_{\mathrm{SM}}^{(131)}$ are the sensitivities of the vector $\vec{A}_{131}$ that represents the magnitude and orientation of the misalignment-induced field-constant coma to the misalignment parameters of the SM. They have similar expressions with $S_{\mathrm{SM}}^{(222)}$ and $T_{\mathrm{SM}}^{(222)}$, respectively, except that the astigmatic aberration coefficient for each individual surface should be replaced with the corresponding coma aberration coefficient.

This step can be interpreted as eliminating the astigmatism by rotating the SM around its coma pivot point. The position of the coma pivot point of the SM can be given by

$$L_{\mathrm{cp}} = -\frac{\Delta\vec{V}_{\mathrm{SM}}}{\Delta\vec{\beta}_{\mathrm{SM}}} = \frac{T_{\mathrm{SM}}^{(131)}}{S_{\mathrm{SM}}^{(131)}}. \tag{40}$$

In effect, even if the on-axis coma is not well compensated at the single-field fine-phasing process, in the multi-field fine-phasing process, we can further use the SM modes to eliminate

the residual coma. In this case, this new alignment strategy can be interpreted as first using the SM modes to eliminate the astigmatism and the residual coma, and then correcting the residual medial focal surface with the tip-tilts of the detector.

In this case, the magnitude and orientation of $\vec{A}_{131}$ should be determined before computing the SM moves to eliminate the astigmatism and coma. The net coma aberration contribution induced by misalignments can be expressed as

$$\Delta W_{\text{Coma}} = -(\vec{A}_{131} \cdot \vec{\rho})(\vec{\rho} \cdot \vec{\rho}). \tag{41}$$

Using the vector multiplication of NAT, Eq. (41) can be rewritten as

$$\Delta W_{\text{Coma}} = \begin{bmatrix} -\vec{A}_{131,x} \\ -\vec{A}_{131,y} \end{bmatrix} \cdot \begin{bmatrix} \rho^3 \cos\phi \\ \rho^3 \sin\phi \end{bmatrix}. \tag{42}$$

Then, by referring to the correspondence between the Seidel coefficients and the Zernike coefficients, we can obtain

$$\begin{bmatrix} \vec{A}_{131,x} \\ \vec{A}_{131,y} \end{bmatrix} = -\Delta \begin{bmatrix} 3C_7 - 3C_{10} - 12C_{14} \\ 3C_8 - 3C_{11} - 12C_{15} \end{bmatrix}. \tag{43}$$

Wavefront measurements at a minimum of one field point can be used to determine $\vec{A}_{131}$. If wavefront measurements at more than one field point are available, $\vec{A}_{131}$ can be determined by solving the over-determined equations.

In this case, Eq. (39) should be replaced with the following expression:

$$-\vec{A}_{131} = S_{\text{SM}}^{(131)} \Delta\vec{V}_{\text{SM}} + T_{\text{SM}}^{(131)} \Delta\vec{\beta}_{\text{SM}}, \tag{44}$$

when determining the SM moves accompanied with Eq. (38).

After using the corrective SM modes to eliminate the astigmatism and control the coma aberration at the same time, we can tilt the detector to correct the residual medial focal surface. This is because the medial focal surface induced by misalignments of the mirrors, which is essentially a kind of field-dependent focus, as shown in Fig. 2, can not only be induced by mirror misalignments, but also can be induced by the tip–tilt misalignments of the detector. This is one of the important differences between the medial focal surface and other aberrations, such as astigmatism and coma, which are nearly unaffected by the misalignments of the detector. The net medial focal surface induced by the tip-tilts of the detector can be expressed as

$$\Delta W_{\text{MFS}} = -2(T_{\text{FP}}\vec{\beta}_{\text{FP}} \cdot \vec{H}) \cdot (\vec{\rho} \cdot \vec{\rho}), \tag{45}$$

where $\vec{\beta}_{\text{FP}}$ represents the tip–tilt of the detector. T_{FP} is a constant, which is expressed as

$$T_{\text{FP}} = -\frac{1}{16F^{\#2}} \cdot f\overline{u}_{\text{PM}}, \tag{46}$$

where $F^{\#}$ represents the F number of the system, f is the focal length, $\overline{u}_{\text{PM}}$ is the paraxial chief ray angle at the PM, and $\vec{H}$ represents the field vector normalized by $\overline{u}_{\text{PM}}$.

Comparing the expression of Eq. (45) with Eqs. (7) and (17), we can recognize that the coefficient T_{FP} can be interpreted as the sensitivity of the vector $\vec{A}_{220M}$ to the tip-tilts of the detector. Therefore, supposing $\Delta\vec{V}_{\text{SM}}$ and $\Delta\vec{\beta}_{\text{SM}}$ are the corrective SM modes for eliminating the field-dependent astigmatism while controlling the coma aberration field, which can be computed with Eqs. (38) and (44), then the corrective tip-tilts of the detector for eliminating the residual medial focal surface can be calculated simultaneously with the following expression:

$$\Delta\vec{\beta}_{\text{FP}} = -\frac{1}{T_{\text{FP}}} \cdot [\vec{A}_{220M} + S_{\text{SM}}^{(220M)} \Delta\vec{V}_{\text{SM}} + T_{\text{SM}}^{(220M)} \Delta\vec{\beta}_{\text{SM}}]. \tag{47}$$

Note that $\vec{A}_{220M}$ is usually measured in λ, while T_{FP} is usually measured in mm. A conversion of measurement units is needed when using Eq. (47) to compute the corrective tip-tilts of the detector.

In practice, the position of the detector may be fixed, and we cannot adjust the tip-tilts of the detector. In this case, we can use some equivalent methods that have similar effects with the tip-tilts of the detector to correct the residual medial focal surface, such as tip-tilting the fold mirror. However, we should note that directly tip-tilting the fold mirror can also introduce transverse displacement of the image. Therefore, in this case, we should not only adjust the tip-tilts of the fold mirror to correct the residual medial focal surface, but also adjust the decenters of the fold mirror to maintain the position of the image at the detector.

We should point out that the system is in a compensated state after the multi-field fine-phasing process using this new strategy, not in the nominal state. However, the system cannot be aligned to the nominal state even using the current alignment strategy either. In effect, under certain perturbation circumstances the system can achieve a high imaging quality even in a compensated state. We will perform Monte Carlo simulations to demonstrate this point in the following part of this section.

C. Simulations

In this part, we will present detailed simulations to demonstrate the efficiency of the new alignment strategy for eliminating the field-dependent aberrations. Specifically, we will compute the corrective SM modes and detector tip-tilts that are needed in this strategy for different misalignment states in different perturbation ranges, and then apply them to the system to see if all three dominant aberrations are well corrected.

We first introduce one set of misalignments of the PM and SM into the simulation software Code V. Utilizing the analytic computation approach presented in this section, the corrective SM modes and the tip-tilts of the detector can be obtained. The specific misalignments of the PM and SM simulated here are presented in rows A and B of Table 4 (the same as Table 1), respectively. The misalignments of the SM after correction with the new strategy, are presented in row C. The tip-tilts of the detector are presented in row D. The medial focal surface, astigmatic, and the coma aberration field before and after correction with the new alignment strategy are shown in Fig. 9.

We can see from Fig. 9 that the two field-dependent aberrations, i.e., medial focal surface and astigmatism, are well eliminated. Besides, the coma aberration field is nearly in a compensated state before correction. After correction, this aberration can further be controlled.

To further demonstrate the efficiency of the new alignment strategy, Monte Carlo simulations will be performed. Three different cases with different misalignment ranges will be

Table 4. Introduced PM and SM Misalignments Before Correction (A and B) and the SM Misalignments (C) and Tip-Tilts of the Detector (D) After Correction

	XDE (mm)	*YDE* (mm)	*ADE* (deg)	*BDE* (deg)
A	0.1113	−0.0996	0.0010	−0.0004
B	−0.0283	−0.1410	0.0060	0.0045
C	0.0602	−0.2292	0.0008	−0.0003
D	\	\	−0.0146	−0.0111

considered in the Monte Carlo simulations. The specific misalignment ranges in each case are the same as those presented in Table 2. For each case, 100 misalignment states will be generated with similar methods to meet the premise that the PM and SM are in a compensated state for the on-axis coma. For each misalignment state, we can compute the corrective SM modes and the tip-tilts of the detector using the new alignment strategy with wavefront measurements at four field points, (−0.1°, 0.1°), (0.1°,0.1°), (−0.1°, −0.1°), and (−0.1°, 0.1°). Then, we apply them to the system. Lastly, we compute the average root mean square (RMS) WFE before and after correction at four off-axis field points, (−0.25°, 0.25°), (0.25°,0.25°), (−0.25°, −0.25°), and (−0.25°, 0.25°). The results are shown in Fig. 10.

We can see that in all three cases, the mean RMS WFE at the four off-axis field points are nearly corrected to the nominal state (the mean RMS WFE at the four field points is 0.0691λ at the nominal state). While there still exists a deviation between the RMS WFE at each of the four field points and the mean value of them, this deviation is rather small ($<0.005\lambda$), and we can consider that the aberrations of the system are well corrected.

Besides, we should also point out that as the perturbation range increases, the magnitude of the tip–tilt of the detector needed will increase correspondingly. Up to some level, the magnitude of the tip–tilt of the detector that is needed may go beyond the adjustment range of the system in practical applications. The magnitudes of the tip–tilt of the detector for the three cases simulated in the previous part of this section are shown in Fig. 11. While in all three cases, the aberrations of the system can be well corrected, as shown in Fig. 10, the magnitude of the tip–tilt of the detector needed in Case 3 is a little larger from an engineering point of view.

Nevertheless, this does not diminish the value of the new strategy. On one hand, after the global alignment commissioning step, course-phasing, and fine-phasing process, most of the misalignments of the system have been controlled. On the other hand, we can directly increase the adjustment range for the tip–tilt of the system and properly decrease the adjustment

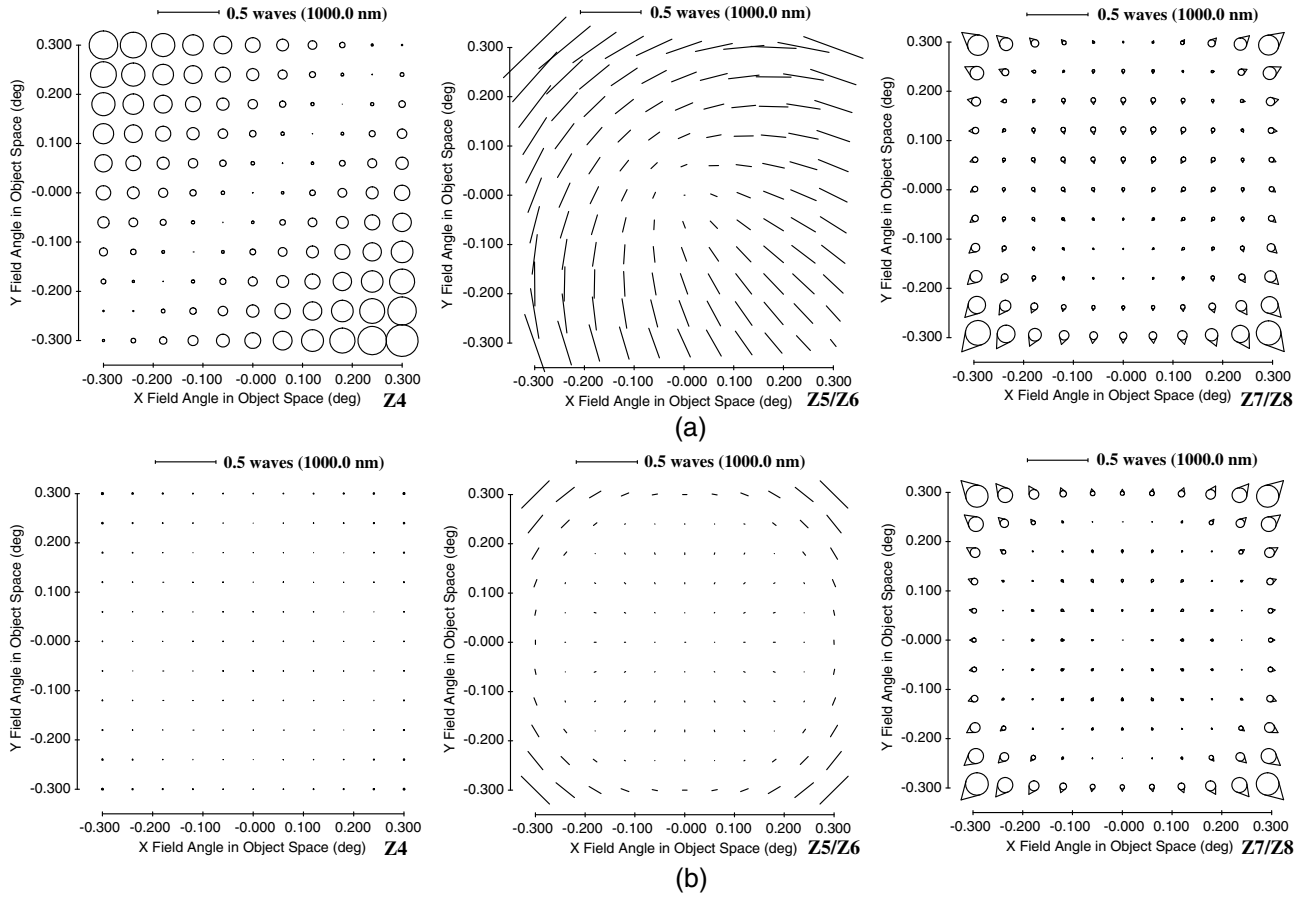

Fig. 9. FFDs for medial focal surface (Z4), astigmatism (Z5/Z6), and coma (Z7/Z8) (a) before and (b) after correction with the new alignment strategy. We can see that the two field-dependent aberrations are well eliminated, and the coma aberration field can also be further controlled.

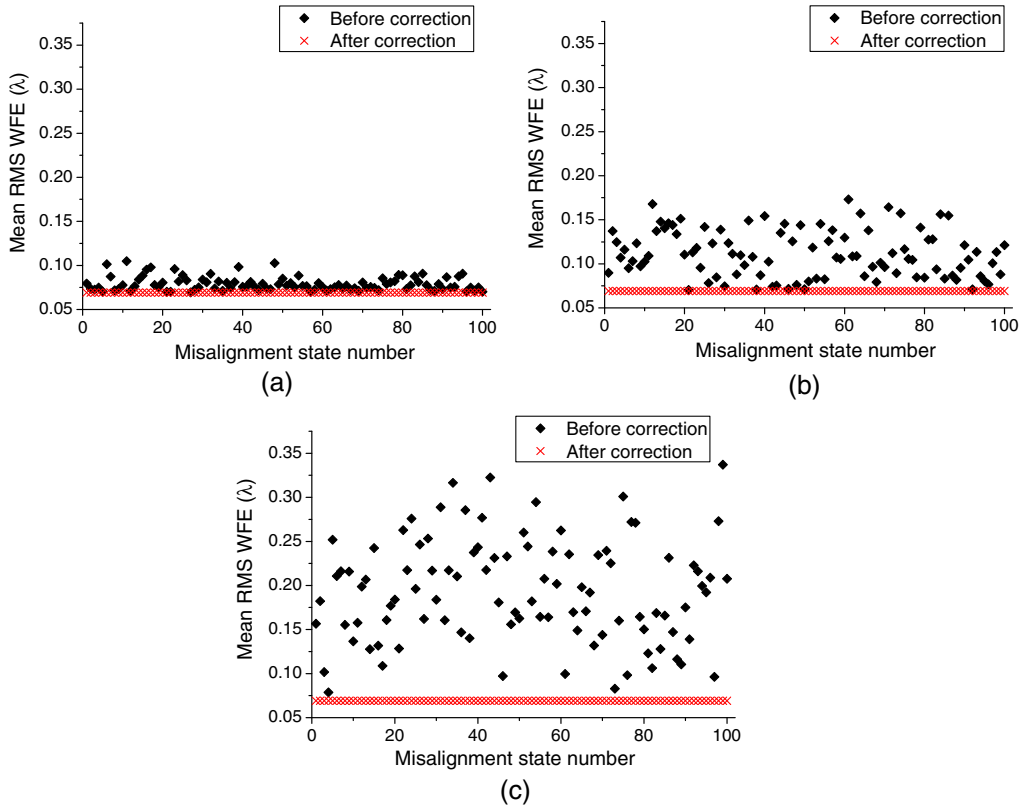

Fig. 10. Mean RMS WFE for the three different cases with increasing perturbation ranges before and after correction with the new alignment strategy. We can see that for all three cases, the aberrations of the system (most of them are field-dependent) are well corrected.

accuracy, because the aberrations of the system are not very sensitive to the tip-tilts of the detector. Besides, the new strategy can also be combined with other alignment strategies, such as the current strategy. Specifically, we can first use the current alignment strategy to partly reduce the magnitudes of the misalignments; after one or two alignment iterations, we can continue to use the new strategy to accelerate the convergence of the alignment process.

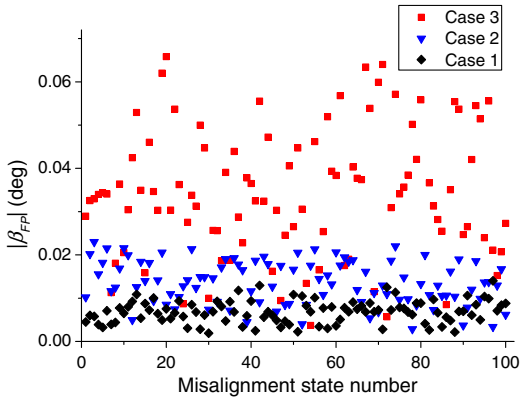

Fig. 11. Magnitudes of the tip–tilt of the detector that are needed to correct the residual medial focal surface for the three different cases presented in Table 2. We can see that as the perturbation range increases, the magnitude of the tip–tilt of the detector will increase correspondingly.

D. Problem of the Current Alignment Strategy for the Case of a Tilted Detector

In this part, we will discuss the problem of the current strategy for the case of a tip-tilted detector to further illustrate the rationality of the new strategy. The detector itself can be in a misaligned state due to the strong transient shock in the launch process of the rocket, and gravity unloading, temperature variation, and platform vibration on orbit. When taking these facts into account, it is very reasonable to use the SM modes to eliminate the astigmatism while maintaining an acceptable WFE on axis, leaving the residual focal surface to be corrected by adjusting the detector. On the contrary, it is very inappropriate to use the SM modes to correct the focal surface induced by the tip–tilt misalignments of the detector.

The tip-tilts of the detector can also introduce some mounts of field-dependent focus, which has the same characteristic as the medial focal surface induced by mirror misalignments. Therefore, in the presence of a tip-tilted detector, it is very likely that a larger magnitude of SM moves is needed to eliminate the two types of field-dependent aberrations, compared to the case of a well-aligned detector. Consequently, a larger on-axis coma will be introduced into the system after applying the corrective SM moves to the system.

To illustrate this problem, Monte Carlo simulations will be performed. For the same 100 misalignment states of the PM and SM utilized in Section 3, on one hand, we calculate the magnitudes of the decenter and tip–tilt misalignments of the SM after correction, using the current strategy when the

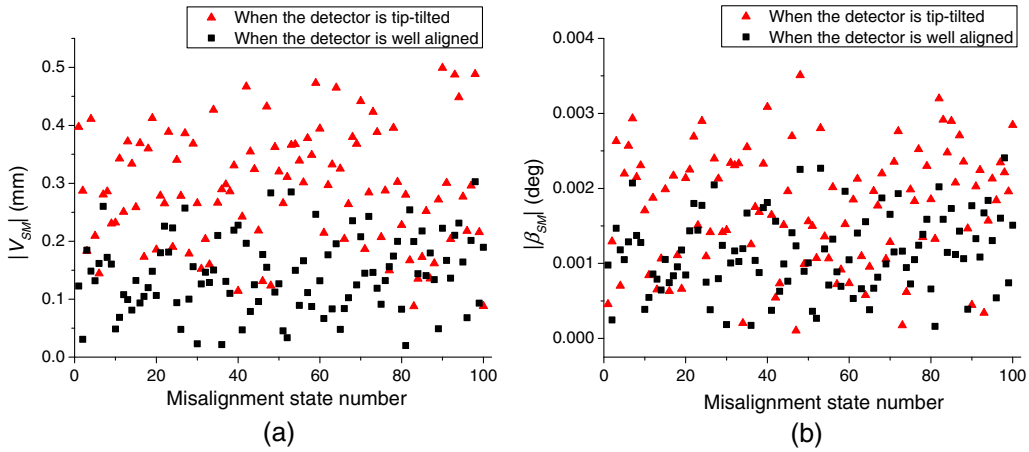

Fig. 12. Magnitudes of the (a) decenter and (b) tip–tilt misalignments of SM after eliminating the field-dependent aberrations with the current strategy for the case of a tip-tilted detector and the case of a well-aligned detector. We can recognize that the magnitudes of the misalignments of the SM after correction for the case of a tip-tilted detector are larger than those for the case of a well-aligned detector.

detector is well aligned; on the other hand, we do the same thing when the detector is misaligned with a 0.05° tip–tilt in a random direction. The magnitudes of the decenter and tip–tilt misalignments of the SM for these two cases are shown in Fig. 12. Here, $|V_{\mathrm{SM}}|$ and $|\beta_{\mathrm{SM}}|$ represent the magnitudes of the decenter and tip–tilt misalignments of the SM, respectively (each measured in mm and degrees, respectively). They are the modulus of the two vectors, $\vec{V}_{\mathrm{SM}}$ and $\vec{\beta}_{\mathrm{SM}}$, i.e., $|V_{\mathrm{SM}}| \equiv \sqrt{XDE_{\mathrm{SM}}^2 + YDE_{\mathrm{SM}}^2}$ and $|\beta_{\mathrm{SM}}| \equiv \sqrt{ADE_{\mathrm{SM}}^2 + BDE_{\mathrm{SM}}^2}$. We can recognize that when the detector is tip-tilted, the magnitudes of the misalignments of the SM after correction are larger than those for the case of a well-aligned detector. Besides, the on-axis coma before and after correction for the case of a tip-tilted detector are shown in Fig. 13. Comparing Fig. 13 with Fig. 8, we can see that a far larger on-axis coma will be induced.

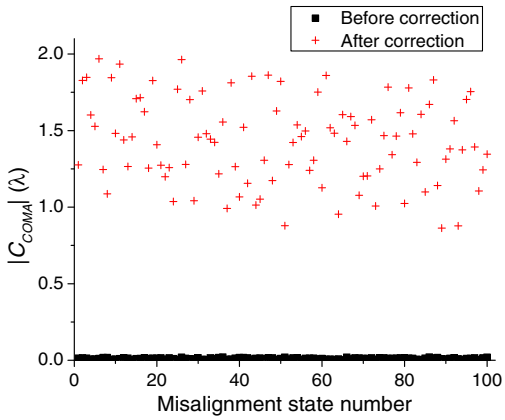

Fig. 13. Magnitudes of the on-axis coma before and after applying the SM moves to correct the field-dependent aberrations with the current strategy in the presence of the tip-tilts of the detector. We can see that in this case a far larger on-axis coma will arise after correction compared to Fig. 8. This indicates that a far larger adjustment of the PM will be needed to reestablish an acceptable WFE, which, unfortunately, may further reintroduce a far larger magnitude of field-dependent aberrations to the system. In this case, it is very likely that the iterative alignment of the PM and SM for eliminating the field-dependent aberrations cannot converge at all.

Consequently, to eliminate this larger field-constant coma, a larger adjustment of the PM will be needed after applying the corrective SM moves. Further, as discussed before, the field-dependent aberrations cannot be controlled simultaneously when re-establishing an acceptable wavefront on axis by adjusting the PM. Consequently, a larger adjustment of the PM can mean that larger field-dependent aberrations will be further reintroduced into the system. In this case, it is very likely that this iterative alignment of the PM and SM for eliminating the field-dependent aberrations cannot converge at all. The worst result is that the magnitudes of the misalignments of the PM and SM are larger and larger during the iterative alignment process of the system using the current alignment strategy.

Therefore, one important premise for the practicability of the current strategy for eliminating the field-dependent aberrations is the good alignment state of the detector. Taking this fact into consideration, we also strongly recommend that the practicability of the current alignment strategy for eliminating the field-dependent aberrations should be revalidated to account for the case of a misaligned detector. In contrast, the

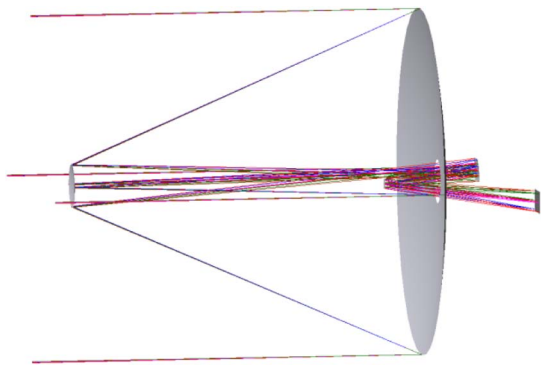

Fig. 14. Optical layout of the simulated TMA telescope, which has similar optical and structural parameters with the JWST.

Table 5. Optical Prescription of the Simulated TMA Telescope

Surface	Type	Conic Constant	Radius (mm)	Thickness (mm)
PM	Conic	−0.9948	−16,287.099	−7170
SM	Conic	−1.8351	−2317.426	7965
TM	Conic	−0.7202	−2702.327	−1845
Fold mirror			Flat	3006.2045
Image			Flat	

Table 6. Third-order Aberration Coefficients of the Simulated TMA Telescope[a]

	PM	SM	TM
$W^{\text{sph}}_{131,j}$	−233.3576	101.2478	−19.9432
$W^{\text{asph}}_{131,j}$	0	113.1192	40.3646
$W^{\text{sph}}_{222,j}$	2.0413	−3.4384	4.5734
$W^{\text{asph}}_{222,j}$	0	3.5926	−6.7610
$W^{\text{sph}}_{220M,j}$	0.2710	2.4693	−4.1268
$W^{\text{asph}}_{220M,j}$	0	3.5930	−2.0571

[a]The aberration coefficients are computed at a field angle of 0.1° at a wavelength of 1 μm.

new strategy can well apply to the case of a tilted detector. The tip-tilts of the detector can hardly affect the astigmatism and coma. We can still use the SM modes to control the astigmatism and coma at the same time. Then, the residual medial focal surface, including those contributed from the tip-tilts of the detector can be corrected by adjusting the tip-tilts of the detector.

5. CONCLUSION

This paper concentrates on the multi-field fine-phasing process in the on-orbit alignment of the JWST-like space telescopes. During the single-field fine-phasing process, an acceptable WFE at the on-axis field point is established. However, there still exist some field-dependent aberrations in the system, which degrades the imaging quality at the off-axis field point. Special alignment strategies are needed to eliminate these field-dependent aberrations in the multi-field fine-phasing process.

Presently, an established alignment strategy directly uses the SM moves to eliminate the two kinds of the field-dependent aberrations, i.e., astigmatism and medial focal surface. A numerical method is used to determine the corrective SM moves at present. To provide an in-depth understanding of this current alignment strategy and answer some basic questions about this strategy, we present an analytic study on this current alignment strategy using the NAT. Monte Carlo simulations demonstrate that this strategy can greatly reduce the field dependency of the WFEs.

However, we can still recognize that there exist some problems in this current alignment strategy. Specifically, a large field-constant coma can be introduced into the system when directly using the SM modes to eliminate the field-dependent aberrations. In this case, once the SM corrections are applied, the PM must be adjusted to reestablish an acceptable wavefront on-axis, which, unfortunately, can further introduce some field-dependent aberrations. The underlying reason for this is that when eliminating the field-dependent aberrations, the WFEs at the on-axis field point are not well controlled simultaneously (when establishing an acceptable wavefront on-axis by adjusting the PM segments during the single-field fine-phasing process, the field-dependent aberrations are not controlled simultaneously either). We can infer that quite a lot of iterations may be required to achieve the adequate alignment of the system. Note that adjusting the PM segments to achieve an acceptable wavefront on-axis after moving the SM is really a complicated and time-consuming work. To this end, we need go back to the global alignment commissioning step and then repeat the coarse-phasing and single-field fine-phasing process. This will reduce the efficiency of the on-orbit alignment of the JWST-like space telescopes and increase the uncertainty and cost of this process.

A new alignment strategy is further proposed to improve the alignment efficiency of the multi-field fine-phasing process based on a deep understanding of the aberration condition of the JWST-like space telescopes before the multi-field fine-phasing process and the problem of the current strategy. In this new strategy, we do not directly use the SM degrees of freedom to eliminate both types of the field-dependent aberrations. On one hand, we adjust the SM to eliminate one of the field-dependent aberrations, astigmatism, while maintaining an acceptable WFE on axis. This can be interpreted as eliminating the astigmatism by rotating the SM around its coma pivot point. Then, the residual medial focal surface, i.e., another field-dependent aberration, can easily be corrected by slightly adjusting the tip–tilt of the detector. One of the main advantages of this strategy is that the segmented PM is no longer needed to readjust in the multi-field fine-phasing process, and therefore improving the alignment efficiency of this process. Detailed simulations are also conducted to demonstrate the efficiency of this new alignment strategy. Besides, some deeper discussions are further presented to illustrate the practicability and rationality of this new strategy, especially when the perfect alignment of the detector cannot be guaranteed.

By presenting an analytic study on the current alignment strategy, revealing the deficiency of this strategy, and further presenting a new one, this paper can not only contribute to an in-depth understanding about eliminating the field-dependent aberrations in the multi-field fine-phasing process, but also present a possibility for improving the efficiency of this process.

APPENDIX A

This Appendix provides the layout, prescription, and third-order aberration coefficients for the TMA telescope simulated in this paper, which have similar optical parameters as the JWST. The layout of this TMA telescope is shown in Fig. 14, and the prescription and third-order aberration coefficients of this TMA telescope are presented in Tables 5 and 6, respectively. Note that these aberrations are a little different from those directly obtained from the optical simulation software. They are computed with a similar method to that presented in Ref. [21].

Funding. National Natural Science Foundation of China (NSFC) (61205143).

REFERENCES

1. M. D. Lallo, "Experience with the Hubble space telescope: 20 years of an archetype," Opt. Eng. **51**, 011011 (2012).
2. H. R. Schember, P. K. Manhart, C. N. Guiar, and J. H. Stevens, "Space infrared telescope facility telescope overview," Proc. SPIE **1540**, 51–62 (1991).
3. P. A. Sabelhaus and J. E. Decker, "An overview of the James Webb Space Telescope (JWST) project," Proc. SPIE **5487**, 550–563 (2004).
4. L. D. Feinberg, B. H. Dean, D. L. Aronstein, C. W. Bowers, W. Hayden, R. G. Lyon, R. Shiri, J. S. Smith, D. S. Acton, L. Carey, A. Contos, E. Sabatke, J. Schwenker, D. Shields, T. Towell, F. Shi, and L. Meza, "TRL-6 for JWST wavefront sensing and control," Proc. SPIE **6687**, 668708 (2007).
5. A. R. Contos, D. S. Acton, A. A. Barto, L. A. Burns, J. Contreras, B. Dean, E. Elliott, L. Feinberg, K. Hansen, B. Hardy, W. Hayden, J. S. Knight, P. A. Lightsey, C. Starr, and J. Sullivan, "Verification of the James Webb Space Telescope (JWST) wavefront sensing and control system," Proc. SPIE **7010**, 70100S (2008).
6. D. Scott Acton, J. Scott Knight, A. Contos, S. Grimaldi, J. Terry, P. Lightsey, A. Barto, B. League, B. Dean, J. S. Smith, C. Bowers, D. Aronstein, L. Feinberg, W. Hayden, T. Comeau, R. Soummer, E. Elliott, M. Perrin, and C. W. Starr, Jr., "Wavefront sensing and controls for the James Webb Space Telescope," Proc. SPIE **8442**, 84423C (2012).
7. D. S. Acton and J. S. Knight, "Multi-field alignment of the James Webb Space Telescope," Proc. SPIE **8442**, 844231 (2012).
8. R. V. Shack and K. P. Thompson, "Influence of alignment errors of a telescope system," Proc. SPIE **251**, 146–153 (1980).
9. K. P. Thompson, "Aberration fields in tilted and decentered optical systems," Ph.D. dissertation (University of Arizona, 1980).
10. K. Thompson, "Description of the third-order optical aberrations of near-circular pupil optical systems without symmetry," J. Opt. Soc. Am. A **22**, 1389–1401 (2005).
11. K. P. Thompson, "Multinodal fifth-order optical aberrations of optical systems without rotational symmetry: spherical aberration," J. Opt. Soc. Am. A **26**, 1090–1100 (2009).
12. K. P. Thompson, "Multinodal fifth-order optical aberrations of optical systems without rotational symmetry: the comatic aberrations," J. Opt. Soc. Am. A **27**, 1490–1504 (2010).
13. K. P. Thompson, "Multinodal fifth-order optical aberrations of optical systems without rotational symmetry: the astigmatic aberrations," J. Opt. Soc. Am. A **28**, 821–836 (2011).
14. T. Schmid, K. P. Thompson, and J. P. Rolland, "Misalignment-induced nodal aberration fields in two-mirror astronomical telescopes," Appl. Opt. **49**, D131–D144 (2010).
15. K. P. Thompson, T. Schmid, and J. P. Rolland, "The misalignment induced aberrations of TMA telescopes," Opt. Express **16**, 20345–20353 (2008).
16. T. Schmid, J. P. Rolland, A. Rakich, and K. P. Thompson, "Separation of the effects of astigmatic figure error from misalignments using nodal aberration theory (NAT)," Opt. Express **18**, 17433–17447 (2010).
17. K. Fuerschbach, J. P. Rolland, and K. P. Thompson, "Extending nodal aberration theory to include mount-induced aberrations with application to freeform surfaces," Opt. Express **20**, 20139–20155 (2012).
18. K. Fuerschbach, J. P. Rolland, and K. P. Thompson, "Theory of aberration fields for general optical systems with freeform surfaces," Opt. Express **22**, 26585–26606 (2014).
19. G. Ju, C. Yan, Z. Gu, and H. Ma, "Aberration fields of off-axis two-mirror astronomical telescopes induced by lateral misalignments," Opt. Express **24**, 24665–24703 (2016).
20. G. Ju, C. Yan, Z. Gu, and H. Ma, "Computation of astigmatic and trefoil figure errors and misalignments for two-mirror telescopes using nodal aberration theory," Appl. Opt. **55**, 3373–3386 (2016).
21. Z. Gu, C. Yan, and Y. Wang, "Alignment of a three-mirror anastigmatic telescope using nodal aberration theory," Opt. Express **23**, 25182–25201 (2015).
22. H. H. Hopkins, *Wave Theory of Aberrations* (Clarendon, 1950).
23. K. P. Thompson, T. Schmid, O. Cakmakci, and J. P. Rolland, "Real-ray-based method for locating individual surface aberration field centers in imaging optical systems without rotational symmetry," J. Opt. Soc. Am. A **26**, 1503–1517 (2009).
24. R. K. Tyson, "Conversion of Zernike aberration coefficients to Seidel and high-order power-series aberration coefficients," Opt. Lett. **7**, 262–264 (1982).
25. R. S. Upton, "Presentation, analysis, and simulation of active alignment strategies for the James Webb Space Telescope," Proc. SPIE **7433**, 743302 (2009).